

The $U(1)_{L_\mu-L_\tau}$ breaking phase transition, muon $g-2$, dark matter, collider and gravitational wave

Jie Wang, Jinghong Ma, Jing Gao, Xiao-Fang Han*, Lei Wang

Department of Physics, Yantai University, Yantai 264005, P. R. China

Abstract

Combining the dark matter and muon $g-2$ anomaly, we study the $U(1)_{L_\mu-L_\tau}$ breaking phase transition, gravitational wave spectra, and the direct detection at the LHC in an extra $U(1)_{L_\mu-L_\tau}$ gauge symmetry extension of the standard model. The new fields includes vector-like leptons (E_1, E_2, N) , $U(1)_{L_\mu-L_\tau}$ breaking scalar S and gauge boson Z' , as well as the dark matter candidate X_I and its heavy partner X_R . A joint explanation of the dark matter relic density and muon $g-2$ anomaly excludes the region where both $\min(m_{E_1}, m_{E_2}, m_N, m_{X_R})$ and $\min(m_{Z'}, m_S)$ are much larger than m_{X_I} . In the parameter space accommodating the DM relic density and muon $g-2$ anomaly, the model can achieve a first-order $U(1)_{L_\mu-L_\tau}$ breaking phase transition, whose strength is sensitive to the parameters of Higgs potential. The corresponding gravitational wave spectra can reach the sensitivity of U-DECIGO. In addition, the direct searches at the LHC impose stringent bound on the mass spectra of the vector-like leptons and dark matter.

PACS numbers: 12.60.Fr, 14.80.Ec, 14.80.Bn

*) Corresponding author. Email address: xfhan@ytu.edu.cn

I. INTRODUCTION

An extra $U(1)_{L_\mu-L_\tau}$ gauge symmetry extension of the standard model (SM) is anomaly-free and naturally breaks Lepton Flavour Universality (LFU) because the $U(1)_{L_\mu-L_\tau}$ gauge boson couples only to $\mu(\tau)$ but not to e . The model was originally formulated by He, Joshi, Lew, and Volkas [1]. Thereafter, this type of $U(1)_{L_\mu-L_\tau}$ model has been modified from its minimal version, and many variants have been proposed in the context of different phenomenological purpose, such as muon $g-2$ anomaly [2–10], dark matter (DM) puzzle [8–18], and $b \rightarrow s\mu^+\mu^-$ anomaly [19–30] etc.

In this paper, we will combine the muon $g-2$ anomaly and DM observables, and examine the $U(1)_{L_\mu-L_\tau}$ breaking phase transition (PT), gravitational wave (GW) signatures, and the exclusion of the LHC direct searches in an extra $U(1)_{L_\mu-L_\tau}$ gauge symmetry extension of SM. The model was proposed by one of our authors in [10], in which the new particles include vector-like leptons (E_1, E_2, N), $U(1)_{L_\mu-L_\tau}$ breaking scalar S and gauge boson Z' , as well as the dark matter candidate X_I and its heavy partner X_R . When the PT is first-order, GW could be generated and detected in current and future GW experiments, such as LISA [31], Taiji [32], TianQin [33], Big Bang Observer (BBO) [34], DECi-hertz Interferometer GW Observatory (DECIGO) [34] and Ultimate-DECIGO (U-DECIGO) [35]. In addition, the null results of the LHC direct searches could exclude some parameter space achieving a first-order PT (FOPT).

II. THE MODEL

Under the local $U(1)_{L_\mu-L_\tau}$, the second (third) generation left-handed lepton doublet and right-handed singlet, $L_\mu, \mu_R, (L_\tau, \tau_R)$, are charged with charge 1 (-1). To obtain the mass of $U(1)_{L_\mu-L_\tau}$ gauge boson Z' , a complex singlet scalar \mathcal{S} is required to break the $U(1)_{L_\mu-L_\tau}$ symmetry. Another complex singlet scalar X with $U(1)_{L_\mu-L_\tau}$ charge is introduced whose lighter component may be as a candidate of DM. Also we add vector-like lepton doublet fields ($E_{L,R}''$) and singlet fields ($E_{L,R}'$) which mediate the X interactions to the muon lepton, and contribute to the muon $g-2$. The quantum numbers of these field under the gauge group $SU(3)_C \times SU(2)_L \times U(1)_Y \times U(1)_{L_\mu-L_\tau}$ are shown in Table I.

TABLE I: The $U(1)_{L_\mu-L_\tau}$ quantum numbers of the new fields.

	$SU(3)_c$	$SU(2)_L$	$U(1)_Y$	$U(1)_{L_\mu-L_\tau}$
X	1	1	0	q_x
\mathcal{S}	1	1	0	$-2q_x$
$E''_{L,R}$	1	2	$-1/2$	$1 - q_x$
$E'_{L,R}$	1	1	-1	$1 - q_x$

The Lagrangian is written as

$$\begin{aligned}
 \mathcal{L} = & \mathcal{L}_{SM} - \frac{1}{4} Z'_{\mu\nu} Z'^{\mu\nu} + g_{Z'} Z'^\mu (\bar{\mu} \gamma_\mu \mu + \bar{\nu}_{\mu_L} \gamma_\mu \nu_{\mu_L} - \bar{\tau} \gamma_\mu \tau - \bar{\nu}_{\tau_L} \gamma_\mu \nu_{\tau_L}) \\
 & + \bar{E}''(i \not{D}) E'' + \bar{E}'(i \not{D}) E' + (D_\mu X^\dagger)(D^\mu X) + (D_\mu \mathcal{S}^\dagger)(D^\mu \mathcal{S}) \\
 & - V + \mathcal{L}_Y.
 \end{aligned} \tag{1}$$

Where $Z'_{\mu\nu} = \partial_\mu Z'_\nu - \partial_\nu Z'_\mu$ is the field strength tensor, D_μ is the covariant derivative, and $g_{Z'}$ is the gauge coupling constant of the $U(1)_{L_\mu-L_\tau}$. V and \mathcal{L}_Y denote the scalar potential and Yukawa interactions.

The scalar potential V containing the SM Higgs parts can be given by

$$\begin{aligned}
 V = & -\mu_h^2 (H^\dagger H) - \mu_S^2 (\mathcal{S}^\dagger \mathcal{S}) + m_X^2 (X^\dagger X) + [\mu X^2 \mathcal{S} + \text{h.c.}] \\
 & + \lambda_H (H^\dagger H)^2 + \lambda_S (\mathcal{S}^\dagger \mathcal{S})^2 + \lambda_X (X^\dagger X)^2 + \lambda_{SX} (\mathcal{S}^\dagger \mathcal{S})(X^\dagger X) \\
 & + \lambda_{HS} (H^\dagger H)(\mathcal{S}^\dagger \mathcal{S}) + \lambda_{HX} (H^\dagger H)(X^\dagger X)
 \end{aligned} \tag{2}$$

with

$$H = \begin{pmatrix} G^+ \\ \frac{1}{\sqrt{2}}(h_1 + v_h + iG) \end{pmatrix}, \mathcal{S} = \frac{1}{\sqrt{2}}(h_2 + v_S + i\omega), X = \frac{1}{\sqrt{2}}(X_R + iX_I). \tag{3}$$

Where $v_h = 246$ GeV and v_S are respectively vacuum expectation values (VeVs) of H and \mathcal{S} , and the X field has no VeV. One can determine the mass parameters μ_h^2 and μ_S^2 of Eq. (2) by the potential minimization conditions,

$$\begin{aligned}
 \mu_h^2 &= \lambda_H v_h^2 + \frac{1}{2} \lambda_{HS} v_S^2, \\
 \mu_S^2 &= \lambda_S v_S^2 + \frac{1}{2} \lambda_{HS} v_h^2.
 \end{aligned} \tag{4}$$

After \mathcal{S} acquires the VeV, the μ term makes the complex scalar X split into two real scalar fields (X_R, X_I), and their masses are

$$\begin{aligned} m_{X_R}^2 &= m_X^2 + \frac{1}{2}\lambda_{HX}v_H^2 + \frac{1}{2}\lambda_{SX}v_S^2 + \sqrt{2}\mu v_S \\ m_{X_I}^2 &= m_X^2 + \frac{1}{2}\lambda_{HX}v_H^2 + \frac{1}{2}\lambda_{SX}v_S^2 - \sqrt{2}\mu v_S. \end{aligned} \quad (5)$$

After the $U(1)_{L_\mu-L_\tau}$ is broken, there is still remnant Z_2 symmetry, which guarantee the lightest component X_I to be as a candidate of DM.

The λ_{HS} and λ_{HX} terms will lead to the couplings of 125 GeV Higgs (h) and DM. To suppress the stringent constraints from the DM direct detection and indirect detection experiments, we simply assume that the $hX_I X_I$ coupling is absent, namely taking $\lambda_{HX} = 0$ and $\lambda_{HS} = 0$. Thus, the 125 GeV Higgs h is purely from h_1 and extra CP-even Higgs S is purely from h_2 . Their masses are given by

$$m_h^2 = 2\lambda_H v_h^2, \quad m_S^2 = 2\lambda_S v_S^2. \quad (6)$$

After \mathcal{S} acquires VeV, the $U(1)_{L_\mu-L_\tau}$ gauge boson Z' obtains a mass,

$$m'_Z = 2g'_Z |q_x| v_S. \quad (7)$$

The Yukawa interactions \mathcal{L}_Y can be written as

$$\begin{aligned} -\mathcal{L}_{Y,\text{mass}} &= m_1 \overline{E'_L} E'_R + m_2 \overline{E''_L} E''_R + \kappa_1 \overline{\mu_R} X E'_L + \kappa_2 \overline{L_\mu} X E''_R \\ &+ \sqrt{2} y_1 \overline{E''_L} H E'_R + \sqrt{2} y_2 \overline{E''_R} H E'_L + \frac{\sqrt{2} m_\mu}{v} \overline{L_\mu} H \mu_R + \text{h.c.} \end{aligned} \quad (8)$$

After the Electroweak symmetry breaking, the vector-like lepton masses are given by

$$M_E = \begin{pmatrix} m_1 & y_2 v_h \\ y_1 v_h & m_2 \end{pmatrix}. \quad (9)$$

By making a bi-unitary transformation with the rotation matrices for the right-handed fields and the left-handed fields,

$$U_L = \begin{pmatrix} c_L & -s_L \\ s_L & c_L \end{pmatrix}, \quad U_R = \begin{pmatrix} c_R & -s_R \\ s_R & c_R \end{pmatrix}, \quad (10)$$

where $c_{L,R}^2 + s_{L,R}^2 = 1$, we can diagonalize the mass matrix for the vector-like lepton,

$$U_L^\dagger M_E U_R = \text{diag}(m_{E_1}, m_{E_2}). \quad (11)$$

The E_1 and E_2 are the mass eigenstates of charged vector-like leptons, and the mass of neutral vector-like lepton N is

$$m_N = m_2 = m_{E_2} c_L c_R + m_{E_1} s_L s_R. \quad (12)$$

The E_1 and E_2 can mediate X_R and X_I interactions to muon lepton,

$$-\mathcal{L}_X \supset \frac{1}{\sqrt{2}}(X_R + iX_I) [\bar{\mu}_R(\kappa_1 c_L E_{1L} - \kappa_1 s_L E_{2L}) + \bar{\mu}_L(\kappa_2 s_R E_{1R} + \kappa_2 c_R E_{2R})] + h.c. , \quad (13)$$

and have the couplings to the 125 GeV Higgs,

$$\begin{aligned} -\mathcal{L}_h \supset & \frac{m_{E_1}(c_L^2 s_R^2 + c_R^2 s_L^2) - 2m_{E_2} s_L c_L s_R c_R}{v_h} h \bar{E}_1 E_1, \\ & + \frac{m_{E_2}(s_L^2 c_R^2 + c_L^2 s_R^2) - 2m_{E_1} s_L c_L s_R c_R}{v_h} h \bar{E}_2 E_2. \end{aligned} \quad (14)$$

III. DARK MATTER AND MUON $g-2$

We fix on $m_h = 125$ GeV, $v_h = 246$ GeV, $q_x = -1$, $\lambda_{HS} = 0$, and $\lambda_{HX} = 0$, and take $g_{Z'}$, $m_{Z'}$, λ_X , λ_{SX} , m_S , m_{X_R} , m_{X_I} , m_{E_1} , m_{E_2} , s_L , s_R , κ_1 , and κ_2 as the free parameters. To maintain the perturbativity, we conservatively choose

$$\begin{aligned} |\lambda_{SX}| &\leq 4\pi, \quad |\lambda_X| \leq 4\pi, \\ -\frac{1}{2} &\leq \kappa_1 \leq \frac{1}{2}, \quad -\frac{1}{2} \leq \kappa_2 \leq \frac{1}{2}, \end{aligned} \quad (15)$$

and take the mixing parameters s_L and s_R as

$$-\frac{1}{\sqrt{2}} \leq s_L \leq \frac{1}{\sqrt{2}}, \quad -\frac{1}{\sqrt{2}} \leq s_R \leq \frac{1}{\sqrt{2}}. \quad (16)$$

The mass parameters are scanned over in the following ranges:

$$\begin{aligned} 60 \text{ GeV} &\leq m_{X_I} \leq 500 \text{ GeV}, \quad m_{X_I} \leq m_{X_R} \leq 500 \text{ GeV}, \\ m_{X_I} &\leq m_{E_1} \leq 500 \text{ GeV}, \quad m_{X_I} \leq m_{E_2} \leq 500 \text{ GeV}, \\ 100 \text{ GeV} &\leq m_{Z'} \leq 500 \text{ GeV}, \quad 100 \text{ GeV} \leq m_S \leq 500 \text{ GeV}. \end{aligned} \quad (17)$$

The mass of neutral vector-like lepton N is a function of m_{E_1} , m_{E_2} , s_L and s_R , and $m_{X_I} < m_N$ is imposed. We require $0 < g_{Z'}/m_{Z'} \leq (550 \text{ GeV})^{-1}$ to be consistent with the bound of the neutrino trident process [36].

The potential stability in Eq. (2) requires the following condition,

$$\begin{aligned}
& \lambda_H \geq 0, \quad \lambda_S \geq 0, \quad \lambda_X \geq 0, \\
& \lambda_{HS} \geq -2\sqrt{\lambda_H \lambda_S}, \quad \lambda_{HX} \geq -2\sqrt{\lambda_H \lambda_X}, \quad \lambda_{SX} \geq -2\sqrt{\lambda_S \lambda_X}, \\
& \sqrt{\lambda_{HS} + 2\sqrt{\lambda_H \lambda_S}} \sqrt{\lambda_{HX} + 2\sqrt{\lambda_H \lambda_X}} \sqrt{\lambda_{SX} + 2\sqrt{\lambda_S \lambda_X}} \\
& + 2\sqrt{\lambda_H \lambda_S \lambda_X} + \lambda_{HS}\sqrt{\lambda_X} + \lambda_{HX}\sqrt{\lambda_S} + \lambda_{SX}\sqrt{\lambda_H} \geq 0.
\end{aligned} \tag{18}$$

The one-loop diagrams with the vector-like lepton can give additional corrections to the oblique parameters (S , T , U), which can be calculated as in Refs. [38–40]. Taking the recent fit results of Ref. [37], we use the following values of S , T , and U ,

$$S = -0.01 \pm 0.10, \quad T = 0.03 \pm 0.12, \quad U = 0.02 \pm 0.11, \tag{19}$$

with the correlation coefficients

$$\rho_{ST} = 0.92, \quad \rho_{SU} = -0.80, \quad \rho_{TU} = -0.93. \tag{20}$$

Also the one-loop diagrams of the charged vector-like leptons E_1 and E_2 can contribute to the $h \rightarrow \gamma\gamma$ decay, and the bound of the diphoton signal strength of the 125 GeV Higgs is imposed [37],

$$\mu_{\gamma\gamma} = 1.11^{+0.10}_{-0.09}. \tag{21}$$

In the model, the dominant corrections to the muon $g - 2$ are from the one-loop diagrams with the vector-like leptons (E_1 , E_2) and scalar fields (X_R and X_I), which are approximately calculated as in Refs. [41–43]

$$\begin{aligned}
\Delta a_\mu = & \frac{1}{32\pi^2} m_\mu (\kappa_1 c_L \kappa_2 s_R H(m_{E_1}, m_{X_R}) - \kappa_1 s_L \kappa_2 c_R H(m_{E_2}, m_{X_R}) \\
& + \kappa_1 c_L \kappa_2 s_R H(m_{E_1}, m_{X_I}) - \kappa_1 s_L \kappa_2 c_R H(m_{E_2}, m_{X_I})),
\end{aligned} \tag{22}$$

where the function

$$H(m_f, m_\phi) = \frac{m_f}{m_\phi^2} \frac{(r^2 - 4r + 2 \log r + 3)}{(r - 1)^3} \tag{23}$$

with $r = \frac{m_f^2}{m_\phi^2}$. The combined average for the muon $g - 2$ with Fermilab E989 [44] and Brookhaven E821 [45], the difference from the SM prediction becomes

$$\Delta a_\mu = a_\mu^{exp} - a_\mu^{SM} = (25.1 \pm 5.9) \times 10^{-10}, \tag{24}$$

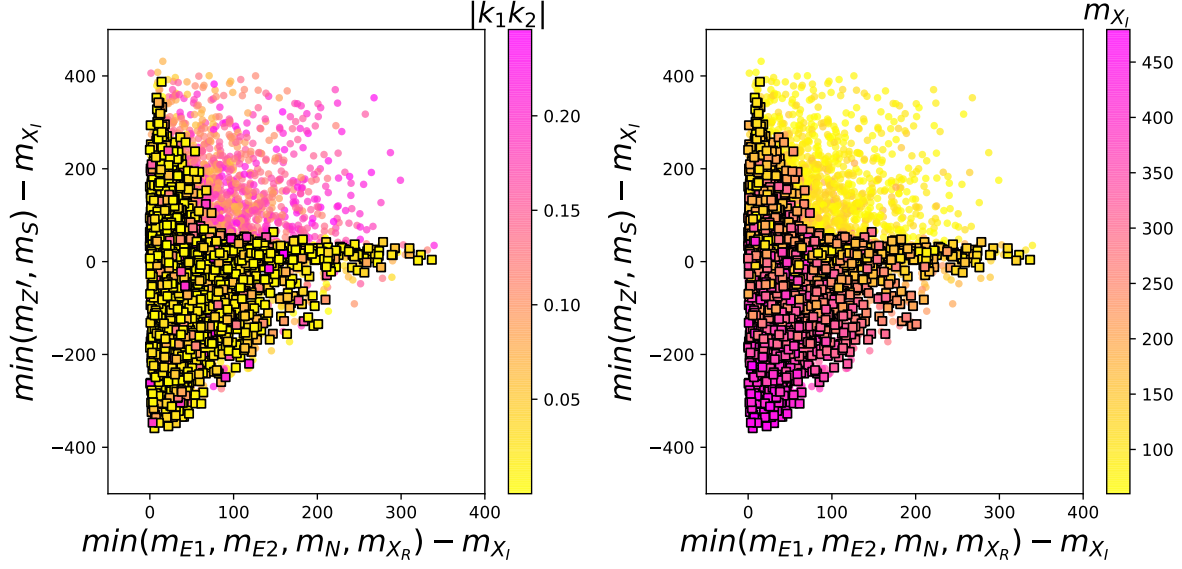


FIG. 1: The surviving samples explaining the DM relic density and muon $g - 2$ anomaly while satisfying the constraints from theory, oblique parameter, and 125 GeV Higgs diphoton signal. The circles and squares are excluded and allowed by the DM relic data.

which shows 4.2σ discrepancy from the SM. Very recently, on August 10, 2023, the E989 experiment at Fermilab released an update regarding the measurement from Run-2 and Run-3 [46]. The new combined value yields a deviation of

$$\Delta a_\mu = a_\mu^{exp} - a_\mu^{SM} = (24.9 \pm 4.8) \times 10^{-10}, \quad (25)$$

which leads to a 5.1σ discrepancy. Whereas the recent lattice calculation [47] and the experiment determination [48] of the hadron vacuum polarization contribution to the muon $g - 2$ point the value closer to the SM prediction, and hence the tension relaxes to a few sigma level.

If kinematically allowed, the DM pair-annihilation processes includes $X_I X_I \rightarrow \mu^+ \mu^-$, $Z' Z'$, SS . In addition, a small mass splitting between the DM and the other new particles (E_1 , E_2 , N , X_R) can lead to coannihilation. The Planck collaboration reported the relic density of cold DM in the universe, $\Omega_c h^2 = 0.1198 \pm 0.0015$ [49], and the theoretical prediction of the model is calculated by `micrOMEGAs-5.2.13` [50].

After imposing the constraints of theory, oblique parameters, and the diphoton signal data of the 125 GeV Higgs, we project the samples accommodating the DM relic density and muon $g - 2$ anomaly within 2σ ranges in Fig. 1. From Fig. 1 we find

that the correct DM relic density can be obtained for most of the parameter region of $\min(m_{E_1}, m_{E_2}, m_N, m_{X_R}) - m_{X_I} < 350$ GeV and -400 GeV $< \min(m_{Z'}, m_S) - m_{X_I} < 400$ GeV. The DM relic density is mainly produced via the DM pair-annihilation processes $X_I X_I \rightarrow Z' Z', SS$ for the region of $\min(m_{Z'}, m_S) < m_{X_I}$, the coannihilation processes for the region of $\min(m_{E_1}, m_{E_2}, m_N, m_{X_R})$ close to m_{X_I} , and $X_I X_I \rightarrow \mu^+ \mu^-$ for the region of both $\min(m_{E_1}, m_{E_2}, m_N, m_{X_R}) > m_{X_I}$ and $\min(m_{Z'}, m_S) > m_{X_I}$. However, once the explanation of muon $g - 2$ anomaly is simultaneously required, most of region of $\min(m_{E_1}, m_{E_2}, m_N, m_{X_R}) > m_{X_I}$ and $\min(m_{Z'}, m_S) > m_{X_I}$ is ruled out. This is because the muon $g - 2$ anomaly favors small interactions between the vector-like leptons and muon mediated by X_I , which leads to $X_I X_I \rightarrow \mu^+ \mu^-$ process to fail to produce the correct DM relic density.

The X_I does not couple to the SM quark, and its couplings to the muon lepton and vector-like leptons are restricted by the muon $g - 2$ anomaly. Therefore, the model can accommodate the bound from the DM direct detection naturally.

IV. $U(1)_{L_\mu-L_\tau}$ BREAKING PHASE TRANSITION

At high temperatures, the global minimum of the finite-temperature effective potential is at the origin, i.e. $SU(2)_L \times U(1)_Y \times U(1)_{L_\mu-L_\tau}$ is unbroken. When the temperature drops, the potential changes and at some point develops a minimum at non-vanishing field values. The PT between the unbroken and the broken phase can proceed in basically two different ways. In a FOPT, at the critical temperature T_C , the two degenerate minima will be at different points in field space, typically with a potential barrier in between. For a second-order (cross-over) transition, the broken and symmetric minimum are not degenerate until they are at the same point in field space. In this paper we focus on a first-order $U(1)_{L_\mu-L_\tau}$ breaking PT.

A. The thermal effective potential

In order to examine PT, we first take h_1, h_2 , and X_r as the field configurations, and obtain the field dependent masses of the scalars (h, S, X_R, X_I), the Goldstone boson (G, ω, G^\pm),

the gauge boson, and fermions. The field dependent masses of scalars are given

$$\hat{m}_{h,S,X_R}^2 = \text{eigenvalues}(\widehat{\mathcal{M}}_P^2) , \quad (26)$$

$$\hat{m}_{G,\omega,X_I}^2 = \text{eigenvalues}(\widehat{\mathcal{M}}_A^2) , \quad (27)$$

$$\hat{m}_{G^\pm}^2 = \lambda_H h_1^2 - \lambda_H v_h^2 , \quad (28)$$

with

$$\begin{aligned} \widehat{\mathcal{M}}_{P11}^2 &= 3\lambda_H h_1^2 - \lambda_H v_h^2 \\ \widehat{\mathcal{M}}_{P22}^2 &= -\lambda_S v_S^2 + 3\lambda_S h_2^2 + \frac{\lambda_{SX}}{2} X_r^2 \\ \widehat{\mathcal{M}}_{P33}^2 &= m_X^2 + \sqrt{2}\mu h_2 + \frac{\lambda_{SX}}{2} h_2^2 + 3\lambda_X X_r^2 \\ \widehat{\mathcal{M}}_{P23}^2 &= \widehat{\mathcal{M}}_{P32}^2 = \sqrt{2}\mu X_r + \lambda_{SX} h_2 X_r \\ \widehat{\mathcal{M}}_{P12}^2 &= \widehat{\mathcal{M}}_{P21}^2 = \widehat{\mathcal{M}}_{P13}^2 = \widehat{\mathcal{M}}_{P31}^2 = 0 \\ \widehat{\mathcal{M}}_{A11}^2 &= \lambda_H h_1^2 - \lambda_H v_h^2 \\ \widehat{\mathcal{M}}_{A22}^2 &= -\lambda_S v_S^2 + \lambda_S h_2^2 + \frac{\lambda_{SX}}{2} X_r^2 \\ \widehat{\mathcal{M}}_{A33}^2 &= m_X^2 - \sqrt{2}\mu h_2 + \lambda_X X_r^2 + \frac{\lambda_{SX}}{2} h_2^2 \\ \widehat{\mathcal{M}}_{A23}^2 &= \widehat{\mathcal{M}}_{A32}^2 = -\sqrt{2}\mu X_r \\ \widehat{\mathcal{M}}_{A12}^2 &= \widehat{\mathcal{M}}_{A21}^2 = \widehat{\mathcal{M}}_{A13}^2 = \widehat{\mathcal{M}}_{A31}^2 = 0. \end{aligned} \quad (29)$$

The field dependent masses of gauge boson are

$$\hat{m}_{W^\pm}^2 = \frac{1}{4}g^2 h_1^2, \quad \hat{m}_Z^2 = \frac{1}{4}(g^2 + g'^2)h_1^2, \quad (30)$$

$$\hat{m}_\gamma^2 = 0, \quad \hat{m}_{Z'}^2 = q_x^2 g_{Z'}^2 (4h_2^2 + X_r^2), \quad (31)$$

The field dependent masses of vector-like lepton are

$$\widehat{\mathcal{M}}_{E1,E2,\mu}^2 = \text{eigenvalues}(\widehat{\mathcal{M}}_E \widehat{\mathcal{M}}_E^T) \quad (32)$$

with

$$\widehat{\mathcal{M}}_E = \begin{pmatrix} m_1 & y_2 h_1 & \kappa_1 X_r \\ y_1 h_1 & m_2 & 0 \\ 0 & \kappa_2 X_r & \frac{m_\mu h_1}{v_h} \end{pmatrix}. \quad (33)$$

For the quarks of SM, we only consider the top quark,

$$\widehat{\mathcal{M}}_t^2 = y_t^2 h_1^2 \quad (34)$$

with $y_t = m_t/v_h$.

In order to examine the $U(1)_{L_\mu-L_\tau}$ breaking PT, we need to study the thermal effective potential V_{eff} in terms of the classical fields (h_1, h_2, X_r) , which is composed of four parts:

$$\begin{aligned} V_{eff}(h_1, h_2, X_r, T) = & V_0(h_1, h_2, X_r) + V_{CW}(h_1, h_2, X_r) + V_{CT}(h_1, h_2, X_r) \\ & + V_T(h_1, h_2, X_r, T) + V_{ring}(h_1, h_2, X_r, T). \end{aligned} \quad (35)$$

V_0 is the tree-level potential, V_{CW} is the Coleman-Weinberg (CW) potential [51], V_{CT} is the counter term, V_T is the thermal correction [52], and V_{ring} is the resummed daisy corrections [53, 54]. In this paper, we calculate V_{eff} in the Landau gauge.

The tree-level potential V_0 in terms of their classical fields (h_1, h_2, X_r) from the Eq. (2),

$$\begin{aligned} V_0(h_1, h_2, X_r) = & -\frac{\mu_h^2}{2} h_1^2 - \frac{\mu_S^2}{2} h_2^2 + \frac{m_X^2}{2} X_r^2 + \frac{\mu}{\sqrt{2}} h_2 X_r^2 \\ & + \frac{\lambda_H}{4} h_1^4 + \frac{\lambda_S}{4} h_2^4 + \frac{\lambda_X}{4} X_r^4 + \frac{\lambda_{SX}}{4} X_r^2 h_2^2. \end{aligned} \quad (36)$$

The CW potential in the $\overline{\text{MS}}$ scheme at 1-loop level has the form [51]:

$$V_{CW}(h_1, h_2, X_r) = \sum_i (-1)^{2s_i} n_i \frac{\hat{m}_i^4(h_1, h_2, X_r)}{64\pi^2} \left[\ln \frac{\hat{m}_i^2(h_1, h_2, X_r)}{Q^2} - C_i \right], \quad (37)$$

where $i = h, S, X_R, X_I, G, \omega, G^\pm, W^\pm, Z, Z', t, E_1, E_2, \mu$, and s_i is the spin of particle i . Q is a renormalization scale, and we take $Q = m_S$. The constants $C_i = \frac{3}{2}$ for scalars or fermions and $C_i = \frac{5}{6}$ for gauge bosons. n_i is the number of degree of freedom,

$$\begin{aligned} n_h = n_S = n_{X_R} = n_{X_I} = n_G = n_\omega = 1 \\ n_{G^\pm} = 2, \quad n_{W^\pm} = 6, \quad n_Z = n_{Z'} = 3 \\ n_t = 12, \quad n_{E_1} = n_{E_2} = n_\mu = 4. \end{aligned} \quad (38)$$

With V_{CW} being included in the potential, the minimization conditions of scalar potential and the CP-even mass matrix will be shifted slightly. To maintain these relations, the counter terms V_{ct} should be added,

$$\begin{aligned} V_{CT} = & \delta m_1^2 h_1^2 + \delta m_2^2 h_2^2 + \delta m_X^2 X_r^2 + \delta \lambda_H h_1^4 + \delta \lambda_S h_2^4 + \delta \lambda_X X_r^4 \\ & + \delta \mu X_r^2 h_2 + \delta \lambda_{SX} h_2^2 X_r^2. \end{aligned} \quad (39)$$

The relevant coefficients are determined by

$$\frac{\partial V_{\text{CT}}}{\partial h_1} = -\frac{\partial V_{\text{CW}}}{\partial h_1}, \quad \frac{\partial V_{\text{CT}}}{\partial h_2} = -\frac{\partial V_{\text{CW}}}{\partial h_2}, \quad \frac{\partial V_{\text{CT}}}{\partial X_r} = -\frac{\partial V_{\text{CW}}}{\partial X_r}, \quad (40)$$

$$\begin{aligned} \frac{\partial^2 V_{\text{CT}}}{\partial h_1 \partial h_1} &= -\frac{\partial^2 V_{\text{CW}}}{\partial h_1 \partial h_1}, & \frac{\partial^2 V_{\text{CT}}}{\partial h_2 \partial h_2} &= -\frac{\partial^2 V_{\text{CW}}}{\partial h_2 \partial h_2}, & \frac{\partial^2 V_{\text{CT}}}{\partial X_r \partial X_r} &= -\frac{\partial^2 V_{\text{CW}}}{\partial X_r \partial X_r}, \\ \frac{\partial^2 V_{\text{CT}}}{\partial h_1 \partial h_2} &= -\frac{\partial^2 V_{\text{CW}}}{\partial h_1 \partial h_2}, & \frac{\partial^2 V_{\text{CT}}}{\partial h_1 \partial X_r} &= -\frac{\partial^2 V_{\text{CW}}}{\partial h_1 \partial X_r}, & \frac{\partial^2 V_{\text{CT}}}{\partial h_2 \partial X_r} &= -\frac{\partial^2 V_{\text{CW}}}{\partial h_2 \partial X_r}, \end{aligned} \quad (41)$$

which are evaluated at the EW minimum of $\{h_1 = v_h, h_2 = v_S, X_r = 0\}$ on both sides. As a result, the VeVs of h_1, h_2, X_r and the CP-even mass matrix will not be shifted. We check that the following relations hold true

$$\frac{\partial^2 V_{\text{CW}}}{\partial h_1 \partial h_2} = 0, \quad \frac{\partial^2 V_{\text{CW}}}{\partial h_1 \partial X_r} = 0. \quad (42)$$

For the left seven equations, there are eight parameters to be fixed, so that one renormalization constant is left for determination. We choose to use $\delta m_1^2, \delta m_2^2, \delta m_X^2, \delta \lambda_H, \delta \lambda_S, \delta \lambda_X, \delta \lambda_{SX}$, and set $\delta \mu = 0$. It is a well-known problem that the second derivative of the CW potential in the vacuum suffers from logarithmic divergences originating from the vanishing Goldstone masses. In order to avoid the problems with infrared divergent Goldstone contributions, we simply remove the Goldstone corrections in the renormalization conditions following the approaches of [55, 56]. This is simply a change of renormalization conditions and the shift it causes in the potential shape is negligible.

The thermal contributions V_T to the potential can be written as [52]

$$V_{\text{th}}(h_1, h_2, X_r, T) = \frac{T^4}{2\pi^2} \sum_i n_i J_{B,F} \left(\frac{\hat{m}_i^2(h_1, h_2, X_r)}{T^2} \right), \quad (43)$$

where $i = h, S, X_R, X_I, G, \omega, G^\pm, W^\pm, Z, Z', t, E_1, E_2, \mu$, and the functions $J_{B,F}$ are

$$J_{B,F}(y) = \pm \int_0^\infty dx x^2 \ln \left[1 \mp \exp \left(-\sqrt{x^2 + y} \right) \right]. \quad (44)$$

Finally, the thermal corrections with resummed ring diagrams are given [53, 54].

$$V_{\text{ring}}(h_1, h_2, X_r, T) = -\frac{T}{12\pi} \sum_i n_i \left[(\bar{M}_i^2(h_1, h_2, X_r, T))^{\frac{3}{2}} - (\hat{m}_i^2(h_1, h_2, X_r, T))^{\frac{3}{2}} \right], \quad (45)$$

where $i = h, S, X_R, X_I, G, \omega, G^\pm, W_L^\pm, Z_L, Z'_L, \gamma_L$. The W_L^\pm, Z_L, Z'_L , and γ_L are the longitudinal gauge bosons with $n_{W_L^\pm} = 2, n_{Z_L} = n_{Z'_L} = n_{\gamma_L} = 1$. The thermal Debye masses

$\bar{M}_i^2(h_1, h_2, X_r, T)$ for the CP-even and CP-odd scalar fields are the eigenvalues of the full mass matrix,

$$\bar{M}_i^2(h_1, h_2, X_r, T) = \text{eigenvalues} \left[\widehat{\mathcal{M}}_X^2(h_1, h_2, X_r) + \Pi_X(T) \right], \quad (46)$$

where Π_X ($X = P, A$) are given by

$$\begin{aligned} (\Pi_{P,A})_{11} &= \left[\frac{9g^2}{2} + \frac{3g'^2}{2} + 12y_t^2 + 4(y_2^2 + y_1^2) + 12\lambda_H \right] \frac{T^2}{24} \\ (\Pi_{P,A})_{22} &= \left[8\lambda_S + 2\lambda_{SX} + 24q_x^2 g_{Z'}^2 \right] \frac{T^2}{24} \\ (\Pi_{P,A})_{33} &= \left[8\lambda_X + 2\lambda_{SX} + 6q_x^2 g_{Z'}^2 + 2\kappa_1^2 + 4\kappa_2^2 \right] \frac{T^2}{24} \\ (\Pi_{P,A})_{12} &= (\Pi_{P,A})_{21} = (\Pi_{P,A})_{13} = (\Pi_{P,A})_{31} = (\Pi_{P,A})_{23} = (\Pi_{P,A})_{32} = 0. \end{aligned} \quad (47)$$

The thermal Debye mass of G^\pm is

$$\bar{M}_{G^+G^-}^2(h_1, h_2, X_r, T) = \lambda_H h_1^2 - \lambda_H v_h^2 + \Pi_{P11}. \quad (48)$$

The Debye masses of longitudinal gauge bosons are

$$\begin{aligned} \bar{M}_{W_L^\pm}^2(h_1, h_2, X_r, T) &= \frac{1}{4}g^2 h_1^2 + \frac{11}{6}g^2 T^2, \\ \bar{M}_{Z_L, \gamma_L}^2(h_1, h_2, X_r, T) &= \frac{1}{8}(g^2 + g'^2) \left(h_1^2 + \frac{22}{3}T^2 \right) \pm \frac{1}{2}\Delta, \\ \bar{M}_{Z'_L}^2(h_1, h_2, X_r, T) &= q_x^2 g_{Z'}^2 (4h_2^2 + X_r^2) + \frac{1}{6}g_{Z'}^2 T^2 [12 - 12q_x + 16q_x^2], \end{aligned} \quad (49)$$

with $\Delta = \sqrt{\left[\frac{1}{4}(g^2 - g'^2) \left(h_1^2 + \frac{22}{3}T^2 \right) \right]^2 + \frac{1}{4}g^2 g'^2 h_1^2}$.

In Fig. 2, we display the scatter plots achieving FOFP and accommodating the DM relic density, muon $g - 2$ anomaly, and various constraints mentioned previously. We observe that the strength of FOPT is sensitive to the parameter λ_S . As λ_S decreases, the critical temperature T_C tends to decrease, and the strength of FOPT tends to increase. We pick out two benchmark points (BPs) to show how the PT happens. The input parameters of BP1 and BP2 are displayed in Table II, and their phase histories are exhibited in Fig. 3 on field configurations versus temperature plane. For the BP1 and BP2, the potential minima at any temperatures always locate at $\langle X_r \rangle = 0$. As the universe cools, a FOPT takes place during which the h_2 acquires a nonzero VeV and the other two fields remain zero. As the temperature continues to decrease, the h_1 starts to develop a nonzero VeV during the second PT which is second-order. Finally, the observed vacuum is obtained at the present temperature.

	λ_{SX}	λ_X	λ_s	$k_1 k_2$	s_L	s_R	gz'	$m_{X_I}(\text{GeV})$
BP1	0.298	1.478	0.067	0.0061	0.113	0.254	0.481	302.9
BP2	0.304	0.337	0.017	-0.0164	-0.280	-0.374	0.319	319.2

	$m_{X_R}(\text{GeV})$	$m_{E_1}(\text{GeV})$	$m_{E_2}(\text{GeV})$	$m_{Z'}(\text{GeV})$	$m_S(\text{GeV})$
BP1	410.2	357.4	454.6	308.4	117.1
BP2	331.4	363.8	469.0	312.3	91.6

TABLE II: Input parameters for the BP1 and BP2.

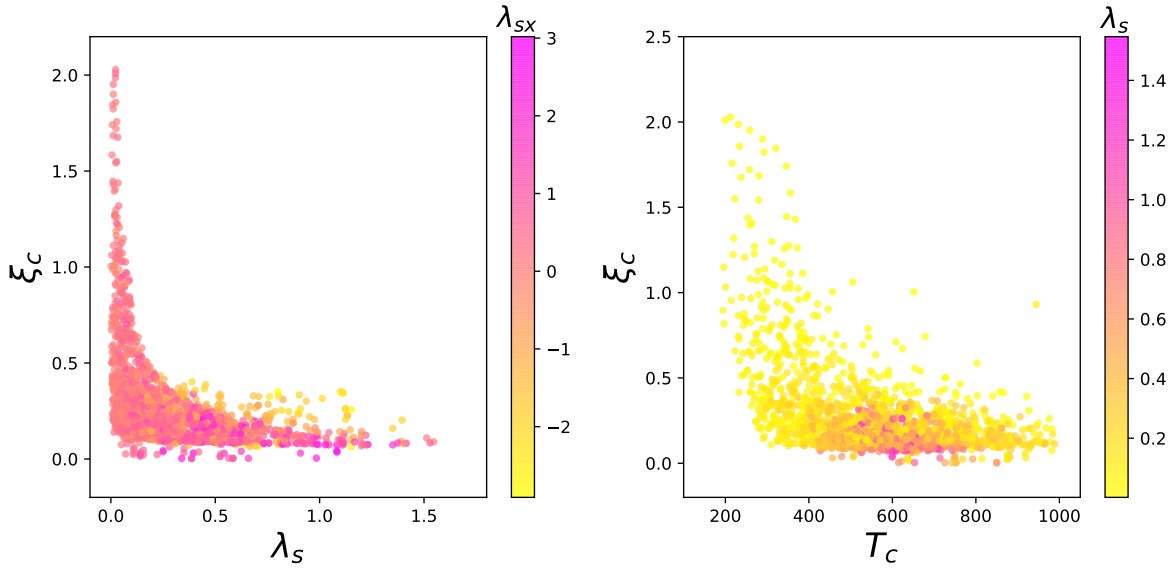


FIG. 2: The surviving samples achieving FOFP and accommodating the DM relic density, muon $g - 2$ anomaly, and various constraints mentioned previously. $\xi_C = \frac{\langle h_2 \rangle}{T_C}$ denotes the strength of the $U(1)_{L_\mu - L_\tau}$ breaking FOPT at the critical temperature T_C .

V. COLLIDER AND GRAVITATIONAL WAVE SIGNATURE

A. Limits from the collider experiments

Since the $U(1)_{L_\mu - L_\tau}$ gauge boson Z' does not couple to quarks, the Z' is rather hard to produce at the LHC. The vector-like leptons are mainly pair produced at the LHC via the electroweak processes mediated by the SM gauge bosons, and the $E_{1,2} \rightarrow \mu X_I$ and $N \rightarrow \nu_\mu X_I$ are main decay modes of vector-like leptons. Thus, we employ the ATLAS analysis of $2\ell + E_T^{miss}$ with 139 fb^{-1} integrated luminosity data to restrict our model [57],

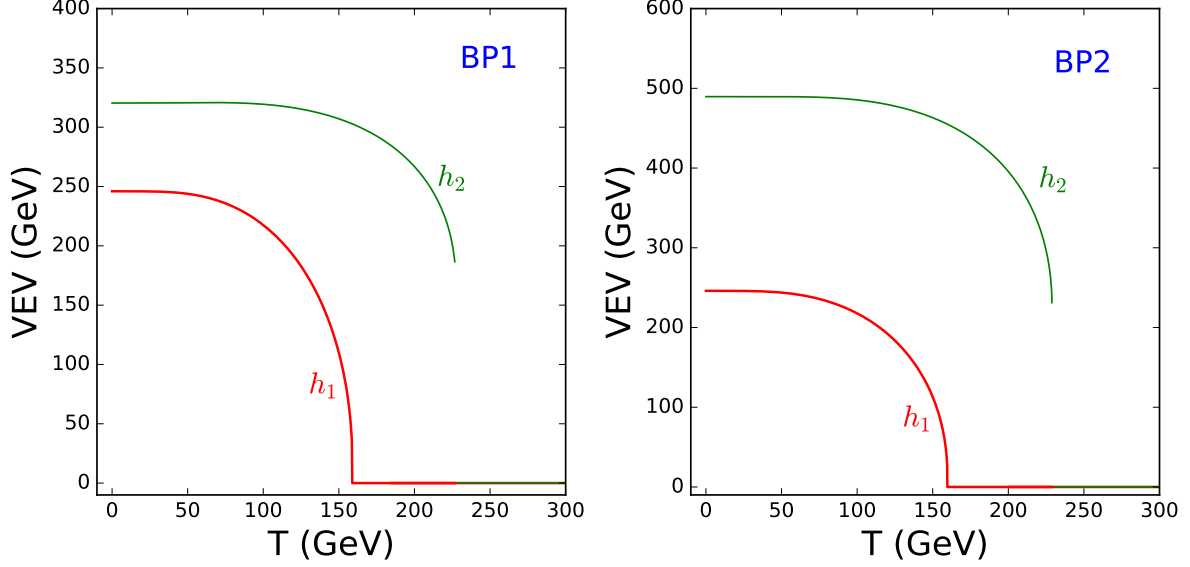


FIG. 3: The phase histories of the BP1 and BP2. The field configuration X_r is not shown as the minima at any temperatures locate at $\langle X_r \rangle = 0$.

which is implemented in the MadAnalysis5 [58–60] with assuming 95% confidence level for the exclusion limit. The simulations for the samples are performed by MG5_aMC-3.3.2 [61] with PYTHIA8 [62] and Delphes-3.2.0 [63].

In Fig. 4, we employ the ATLAS analysis of $2\ell + E_T^{miss}$ at the LHC to restrict the parameter space which has been satisfied by the DM relic density, muon $g-2$, FOPT, and various constraints discussed above. Fig. 4 indicates that the DM mass is allowed to be as low as 100 GeV when the value of $\min(m_{E_1}, m_{E_2}) - m_{X_I}$ is small. This is because the muon from the vector-like lepton decay has soft energy, and its detection efficiency is decreased at the LHC. As the DM mass increase, the value of $\min(m_{E_1}, m_{E_2}) - m_{X_I}$ increases, and the lightest charged vector-like lepton is allowed to have a more large mass.

B. Gravitational wave signature

Stochastic GWs are produced during a FOPT via bubble collision, sound waves in the plasma and the magneto-hydrodynamics turbulence. Since most of the PT energy is pumped into the surrounding fluid shells, making sound waves the dominant contribution to GWs, we will focus on the GW spectrum from the sound waves in the plasma.

The sound wave spectra can be expressed as functions of two FOPT parameters β and

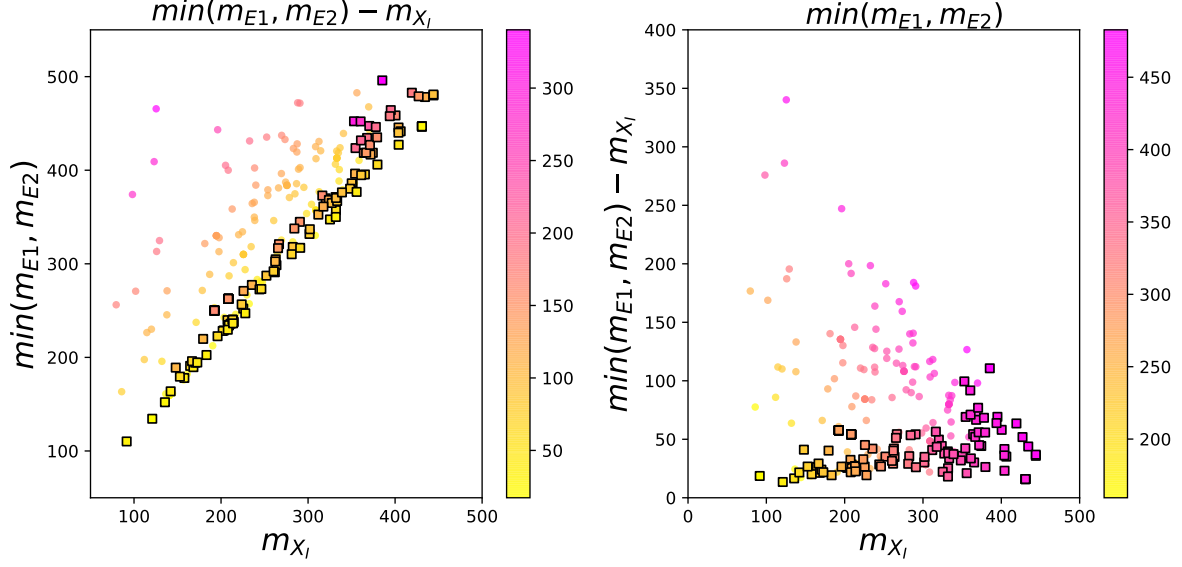


FIG. 4: All the samples achieve FOFP and accommodate the DM relic density, muon $g-2$ anomaly, and various constraints mentioned previously. The circles and squares are excluded and allowed by the direct searches for $2\ell + E_T^{miss}$ at the LHC.

α ,

$$\frac{\beta}{H_n} = T \frac{d(S_3(T)/T)}{dT} \Big|_{T=T_n}, \quad \alpha = \frac{\Delta\rho}{\rho_R} = \frac{\Delta\rho}{\pi^2 g_* T_n^4/30}. \quad (50)$$

Where H_n is the Hubble parameter at the nucleation temperature T_n , and g_* is the effective number of relativistic degrees of freedom. β characterizes roughly the inverse time duration of the strong first-order PT, and α is defined as the vacuum energy released from the PT normalized by the total radiation energy density ρ_R at T_n .

The GW spectrum from the sound waves can be expressed by [64]

$$\begin{aligned} \Omega_{\text{sw}} h^2 &= 2.65 \times 10^{-6} \left(\frac{H_n}{\beta} \right) \left(\frac{\kappa_v \alpha}{1 + \alpha} \right)^2 \left(\frac{100}{g_*} \right)^{1/3} v_w \\ &\times \left(\frac{f}{f_{\text{sw}}} \right)^3 \left(\frac{7}{4 + 3(f/f_{\text{sw}})^2} \right)^{7/2} \Upsilon(\tau_{\text{sw}}), \end{aligned} \quad (51)$$

where v_w is the wall velocity, and we take $v_w = c_s = \sqrt{1/3}$ with c_s being the sound velocity. f_{sw} is the present peak frequency of the spectrum,

$$f_{\text{sw}} = 1.9 \times 10^{-5} \frac{1}{v_w} \left(\frac{\beta}{H_n} \right) \left(\frac{T_n}{100 \text{ GeV}} \right) \left(\frac{g_*}{100} \right)^{1/6} \text{ Hz}. \quad (52)$$

The κ_v is the fraction of latent heat transformed into the kinetic energy of the fluid [65],

$$\kappa_v \simeq \frac{\alpha^{2/5}}{0.017 + (0.997 + \alpha)^{2/5}}. \quad (53)$$

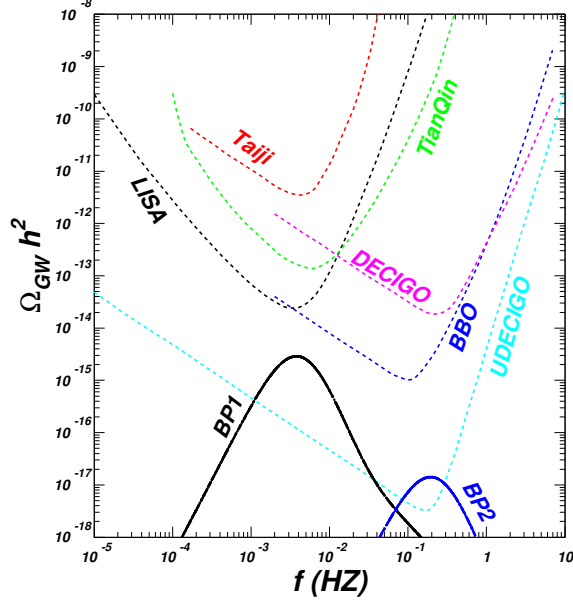


FIG. 5: Gravitational wave spectra for the BP1 and BP2.

The suppression factor of Eq. (51) [66]

$$\Upsilon(\tau_{sw}) = 1 - \frac{1}{\sqrt{1 + 2\tau_{sw}H_n}}, \quad (54)$$

appears due to the finite lifetime τ_{sw} of the sound waves [67, 68],

$$\tau_{sw} = \frac{\tilde{v}_W(8\pi)^{1/3}}{\beta\bar{U}_f}, \quad \bar{U}_f^2 = \frac{3}{4} \frac{\kappa_v \alpha}{1 + \alpha}. \quad (55)$$

We calculate GW spectra for thousands of parameter points accommodating the muon $g-2$, DM relic density, and the exclusion limits of the LHC direct searches, and find that all the peak strengths are below the sensitivity curve of BBO. About 10 percent of the survived points can generate U-DECIGO sensitive gravitational wave, including BP1 and BP2. These points favor a small λ_S for which the strength of FOPT tends to have a large value. The GW spectra of BP1 and BP2 are shown along with expected sensitivities of various future interferometer experiments in Fig. 5. The lowest peak frequency is 0.003 HZ from BP1, and the highest peak frequency is 0.2 HZ from BP2.

VI. CONCLUSION

We study an extra $U(1)_{L_\mu-L_\tau}$ gauge symmetry extension of the standard model by considering the dark matter, muon $g-2$ anomaly, the $U(1)_{L_\mu-L_\tau}$ breaking PT, GW spectra, and

the bound from the direct detection at the LHC. We obtained the following observations: (i) A joint explanation of the dark matter relic density and muon $g - 2$ anomaly rules out the region where both $\min(m_{E_1}, m_{E_2}, m_N, m_{X_R})$ and $\min(m_{Z'}, m_S)$ are much larger than m_{X_I} . (ii) A first-order $U(1)_{L_\mu - L_\tau}$ breaking PT can be achieved in the parameter space explaining the DM relic density and muon $g - 2$ anomaly simultaneously, and the corresponding gravitational wave spectra can reach the sensitivity of U-DECIGO. (iii) The mass spectra of the vector-like leptons and dark matter are stringently restricted by the direct searches at the LHC.

Acknowledgment

This work was supported by the National Natural Science Foundation of China under grant 11975013.

-
- [1] X. G. He, G. C. Joshi, H. Lew and R. R. Volkas, “New- Z' phenomenology”, Phys. Rev. D **43**, (1991) 22–24.
 - [2] E. Ma, D. P. Roy and S. Roy, Gauged $L_\mu - L_\tau$ with large muon anomalous magnetic moment and the bimaximal mixing of neutrinos, Phys. Lett. B **525**, (2002) 101–106.
 - [3] S. Baek, N. G. Deshpande, X. G. He and P. Ko, Muon anomalous $g-2$ and gauged $L_\mu - L_\tau$ models, Phys. Rev. D **64**, (2001) 055006.
 - [4] J. Heeck and W. Rodejohann, Gauged $L_\mu - L_\tau$ Symmetry at the Electroweak Scale, Phys. Rev. D **84**, (2011) 075007.
 - [5] K. Harigaya, T. Igari, M. M. Nojiri, M. Takeuchi and K. Tobe, Muon $g-2$ and LHC phenomenology in the $L_\mu - L_\tau$ gauge symmetric model, JHEP **03**, (2014) 105.
 - [6] W. Altmannshofer, C.-Y. Chen, P. S. Bhupal Dev and A. Soni, Lepton flavor violating Z' explanation of the muon anomalous magnetic moment, Phys. Lett. B **762**, (2016) 389–398.
 - [7] H. Banerjee, P. Byakti and S. Roy, Supersymmetric gauged $U(1)_{L_\mu - L_\tau}$ model for neutrinos and the muon $(g - 2)$ anomaly, Phys. Rev. D **98**, (2018) 075022.
 - [8] A. Biswas, S. Choubey and S. Khan, Neutrino Mass, Dark Matter and Anomalous Magnetic Moment of Muon in a $U(1)_{L_\mu - L_\tau}$ Model, JHEP **09**, (2016) 147.

- [9] A. Biswas, S. Choubey and S. Khan, FIMP and Muon $(g - 2)$ in a $U(1)_{L_\mu - L_\tau}$ Model, JHEP **02**, (2017) 123.
- [10] Q. Zhou, X. F. Han and L. Wang, The CDF W-mass, muon $g - 2$, and dark matter in a $U(1)_{L_\mu - L_\tau}$ model with vector-like leptons, Eur. Phys. J. C **82**, 1135 (2022).
- [11] F. Costa, S. Khan and J. Kim, “A two-component dark matter model and its associated gravitational waves,” JHEP **06**, 026 (2022)
- [12] E. J. Chun, A. Das, J. Kim and J. Kim, “Searching for flavored gauge bosons,” JHEP **02**, 093 (2019)
- [13] S. Baek and P. Ko, Phenomenology of $U(1)_{L_\mu - L_\tau}$ charged dark matter at PAMELA and colliders, JCAP **0910**, (2009) 011.
- [14] M. Das and S. Mohanty, Leptophilic dark matter in gauged $L_\mu - L_\tau$ extension of MSSM, Phys. Rev. D **89**, (2014) 025004.
- [15] S. Patra, S. Rao, N. Sahoo and N. Sahu, Gauged $U(1)_{L_\mu - L_\tau}$ model in light of muon $g - 2$ anomaly, neutrino mass and dark matter phenomenology, Nucl. Phys. B **917**, (2017) 317-336.
- [16] A. Biswas, S. Choubey, L. Covi and S. Khan, Explaining the 3.5 keV X-ray Line in a $L_\mu - L_\tau$ Extension of the Inert Doublet Model, JCAP **1802**, (2018) 002.
- [17] P. Foldenauer, Light dark matter in a gauged $U(1)_{L_\mu - L_\tau}$ model, Phys. Rev. D **99**, (2019) 035007.
- [18] N. Okada and O. Seto, “Inelastic extra $U(1)$ charged scalar dark matter,” Phys. Rev. D **101**, (2020) 023522.
- [19] A. Crivellin, G. D’Ambrosio and J. Heeck, Phys. Rev. Lett. **114**, (2015) 151801.
- [20] W. Altmannshofer, S. Gori, S. Profumo and F. S. Queiroz, JHEP **12**, (2016) 106.
- [21] C.-H. Chen and T. Nomura, Phys. Lett. B **777**, (2018) 420–427.
- [22] S. Baek, Phys. Lett. B **781**, (2018) 376–382.
- [23] W. Altmannshofer, S. Gori, M. Pospelov and I. Yavin, Phys. Rev. D **89**, (2014) 095033.
- [24] P. Arnan, L. Hofer, F. Mescia and A. Crivellin, JHEP **04**, (2017) 043.
- [25] S. Singirala, S. Sahoo and R. Mohanta, Exploring dark matter, Phys. Rev. D **99**, (2019) 035042.
- [26] P. T. P. Hutaeruk, T. Nomura, H. Okada and Y. Orikasa, Phys. Rev. D **99**, (2019) 055041.
- [27] A. Biswas, A. Shaw, JHEP **05**, (2019) 165.
- [28] Z.-L. Han, R. Ding, S.-J. Lin, B. Zhu, Eur. Phys. Jour. C **79**, (2019) 1007.

- [29] A. S. Joshipura, N. Mahajan, K. M. Patel, JHEP **03**, (2020) 001.
- [30] W. Chao, H. Wang, L. Wang and Y. Zhang, “Dark matter, Z' , vector-like quark at the LHC and $b \rightarrow s\mu\mu$ anomaly,” Chin. Phys. C **45**, 083105 (2021).
- [31] LISA Collaboration, H. Audley et al., Laser Interferometer Space Antenna, arXiv:1702.00786.
- [32] X. Gong et al., Descope of the ALIA mission, J. Phys. Conf. Ser. **610**, 012011 (2015).
- [33] TianQin Collaboration, J. Luo et al., TianQin: a space-borne gravitational wave detector, Class. Quant. Grav. **33**, 035010 (2016).
- [34] K. Yagi and N. Seto, Detector configuration of DECIGO/BBO and identification of cosmological neutron-star binaries, Phys. Rev. D **83**, 044011 (2011).
- [35] H. Kudoh, A. Taruya, T. Hiramatsu, and Y. Himemoto, Detecting a gravitational-wave background with next-generation space interferometers, Phys. Rev. D **73**, 064006 (2006).
- [36] W. Altmannshofer, S. Gori, M. Pospelov and I. Yavin, “Neutrino trident production: a powerful probe of new physics with neutrino beams.”, Phys. Rev. Lett. **113**, 091801 (2014).
- [37] P. A. Zyla et al. [Particle Data Group], Review of Particle Physics, PTEP **2020**, 083C01 (2020).
- [38] M. E. Peskin and T. Takeuchi, “New constraint on a strongly interacting Higgs sector”, Phys. Rev. Lett. **65**, 964 (1990).
- [39] M.-C. Chen, S. Dawson, “One-loop radiative corrections to the ρ parameter in the littlest Higgs model”, Phys. Rev. D **70**, (2004) 015003.
- [40] S. K. Garg, C. S. Kim, “Vector like leptons with extended Higgs sector”, arXiv:1305.4712.
- [41] R. Dermisek, A. Raval, “Explanation of the muon $g-2$ anomaly with vectorlike leptons and its implications for Higgs decays”, Phys. Rev. D **88**, (2013) 013017.
- [42] J. Kawamura, S. Raby, A. Trautner, “Complete vectorlike fourth family and new $U(1)'$ for muon anomalies”, Phys. Rev. D **100**, (2019) 055030.
- [43] F. Jegerlehner, A. Nyffeler, “The Muon $g-2$ ”, Phys. Rept. **477**, (2009) 1–110.
- [44] B. Abi *et al.* [Fermilab Collaboration], “Measurement of the Positive Muon Anomalous Magnetic Moment to 0.46 ppm”, Phys. Rev. Lett. **126**, (2021) 141801.
- [45] Muon $g-2$ Collaboration, “Precise measurement of the positive muon anomalous magnetic moment”, Phys. Rev. Lett. **86**, (2001) 2227; “Final Report of the Muon E821 Anomalous Magnetic Moment Measurement at BNL”, Phys. Rev. D **73**, (2006) 072003.
- [46] J. Mott et al., New results from the Muon $g-2$ experiment at Fermilab,

<https://indico.fnal.gov/event/60738/>.

- [47] S. Borsanyi et al., Leading-order hadronic vacuum polarization contribution to the muon magnetic moment from lattice QCD, arXiv:2002.12347.
- [48] CMD-3 Collaboration, F. V. Ignatov et al., Measurement of the $e^+e^- \rightarrow \pi^+\pi^-$ cross section from threshold to 1.2 GeV with the CMD-3 detector, arXiv:2302.08834.
- [49] Planck Collaboration, “Planck 2015 results. XXVII. The Second Planck Catalogue of Sunyaev-Zeldovich Sources”, *Astron. Astrophys. A* **27**, 594 (2016).
- [50] G. Belanger, F. Boudjema, A. Pukhov, A. Semenov, “micrOMEGAs-3: A program for calculating dark matter observables”, *Comput. Phys. Commun.* **185**, 960-985 (2014).
- [51] S. R. Coleman and E. J. Weinberg, Radiative Corrections as the Origin of Spontaneous Symmetry Breaking, *Phys. Rev. D* **7**, 1888 (1973).
- [52] L. Dolan and R. Jackiw, Symmetry Behavior at Finite Temperature, *Phys. Rev. D* **9**, 3320 (1974).
- [53] P. B. Arnold and O. Espinosa, The Effective potential and first order phase transitions: Beyond leading-order, *Phys. Rev. D* **47**, 3546 (1993) [Erratum: *Phys. Rev. D* **50**, 6662 (1994)].
- [54] R. R. Parwani, Resummation in a hot scalar field theory, *Phys. Rev. D* **45**, 4695 (1992).
- [55] J. M. Cline, K. Kainulainen and M. Trott, “Electroweak Baryogenesis in Two Higgs Doublet Models and B meson anomalies,” *JHEP* **1111**, 089 (2011).
- [56] J. R. Espinosa, T. Konstandin and F. Riva, “Strong Electroweak Phase Transitions in the Standard Model with a Singlet,” *Nucl. Phys. B* **854** (2012), 592-630.
- [57] ATLAS Collaboration, “Search for electroweak production of charginos and sleptons decaying into final states with two leptons and missing transverse momentum in $\sqrt{s} = 13$ TeV pp collisions using the ATLAS detector”, *Eur. Phys. Jour. C* **80**, (2020) 123.
- [58] E. Conte, B. Fuks, “Confronting new physics theories to LHC data with MADANALYSIS 5”, *Int. J. Mod. Phys. A* **33**, (2018) 1830027.
- [59] J. Y. Araz, M. Frank and B. Fuks, “Reinterpreting the results of the LHC with MadAnalysis 5: uncertainties and higher-luminosity estimates”, *Eur. Phys. Jour. C* **80**, (2020) 531.
- [60] J. Y. Araz, B. Fuks and G. Polykratis, “Simplified fast detector simulation in MADANALYSIS 5”, *Eur. Phys. Jour. C* **81**, 329 (2021).
- [61] J. Alwall *et al.*, “The automated computation of tree-level and next-to-leading order differential cross sections, and their matching to parton shower simulations”, *JHEP* **1407**, (2014)

079.

- [62] P. Torrielli and S. Frixione, “Matching NLO QCD computations with PYTHIA using MC@NLO”, *JHEP* **1004**, (2010) 110.
- [63] J. de Favereau *et al.* [DELPHES 3 Collaboration], “DELPHES 3, A modular framework for fast simulation of a generic collider experiment”, *JHEP* **1402**, (2014) 057.
- [64] M. Hindmarsh, S. J. Huber, K. Rummukainen, and D. J. Weir, Numerical simulations of acoustically generated gravitational waves at a first order phase transition, *Phys. Rev. D* **92**, 123009 (2015).
- [65] M. Maziashvili, *JCAP* **1006**, 028 (2010).
- [66] H.-K. Guo, K. Sinha, D. Vagie and G. White, Phase Transitions in an Expanding Universe: Stochastic Gravitational Waves in Standard and Non-Standard Histories, *JCAP* **01**, 001 (2021).
- [67] J. Ellis, M. Lewicki and J. M. No, Gravitational waves from first-order cosmological phase transitions: lifetime of the sound wave source, *JCAP* **07**, 050 (2020).
- [68] X. Wang, F. P. Huang and X. Zhang, Phase transition dynamics and gravitational wave spectra of strong first-order phase transition in supercooled universe, *JCAP* **05**, 045 (2020).